Inorganic Chemistry

Article

pubs.acs.org/IC

Homoleptic Lanthanide 1,2,3-Triazolates $^{2-3}_{\infty}[Ln(Tz^*)_3]$ and Their Diversified Photoluminescence Properties

J.-Christoph Rybak,[†] Larissa V. Meyer,[†] Julian Wagenhöfer,[‡] Gerhard Sextl,[‡] and Klaus Müller-Buschbaum*,[†]

[†]Institut für Anorganische Chemie, Universität Würzburg, Am Hubland, D-97074 Würzburg, Germany

[‡]Lehrstuhl für Chemische Technologie der Materialsynthese, Universität Würzburg, Röntgenring 11, D-97070 Würzburg, Germany

Supporting Information

ABSTRACT: The series of homoleptic lanthanide 1,2,3-triazolates $^{3}_{\infty}[Ln(Tz^*)_3]$ (Ln^{3+} = lanthanide cation, Tz^{*-} = 1,2,3-triazolate anion, $C_2H_2N_3^-$) is completed by synthesis of the three-dimensional (3D) frameworks with Ln = La, Ce, Pr, Nd, and Sm, and characterization by X-ray powder diffraction, differential thermal analysis-thermogravimetry (DTA/TG) investigations and molecular vibration analysis. In addition, α-$^{2}_{\infty}[Sm(Tz^*)_3]$, a two-dimensional polymorph of 3D β-$^{3}_{\infty}[Sm(Tz^*)_3]$, is presented including the single crystal structure. The 3D lanthanide triazolates form an isotypic series of the formula $^{3}_{\infty}[Ln(Tz^*)_3]$ ranging from La to Lu, with the exception of Eu, which forms a mixed valent metal organic framework (MOF) of different structure and the constitution $^{3}_{\infty}[Eu(Tz^*)_{6+x}(Tz^*H)_{2-x}]$. The main focus of this work is put on the investigation of the photoluminescence behavior of lanthanide 1,2,3-triazolates $^{3}_{\infty}[Ln(Tz^*)_3]$ and illuminates that six different luminescence phenomena can be found for one series of isotypic compounds. The luminescence behavior of the majority of these compounds is based on the photoluminescence properties of the organic linker molecules. Differing properties are observed for $^{3}_{\infty}[Yb(Tz^*)_3]$, which exhibits luminescence properties based on charge transfer transitions between the linker and Yb^{3+} ions, and for $^{3}_{\infty}[Ce(Tz^*)_3]$ and $^{3}_{\infty}[Tb(Tz^*)_3]$, in which the luminescence properties are a combination of the ligand and the lanthanide metal. In addition, strong inner-filter effects are found in the ligand emission bands that are attributed to reabsorption of the emitted light by the trivalent lanthanide ions. Antenna effects of varying efficiency are present indicated by the energy being transferred to the lanthanide ions subsequent to excitation of the ligand. $^{3}_{\infty}[Ce(Tz^*)_3]$ shows a 5d-4f induced intense blue emission upon excitation with UV light, while $^{3}_{\infty}[Tb(Tz^*)_3]$ shows emission in the green region of the visible spectrum, which can be identified with 4f-4f-transitions typical for Tb^{3+} ions.

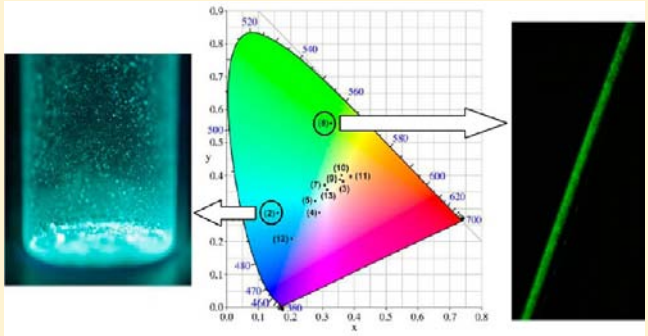

INTRODUCTION

When the topic of metal organic frameworks (MOFs) is discussed, interest often focuses on porous materials originating from the chemistry of transition metals and carboxylic acids.[1] Their porosity based properties, such as gas storage[2] and separation,[3] are the area of main scientific interest. It is widely unacknowledged that a class of dense organic−inorganic hybrid materials exists that are also known as "*dense MOFs*".[4] Even if this class of materials is not eligible to exhibit porosity based properties, they can provide equally interesting qualities, for example, concerning their magnetic behavior,[5] conductivity,[6] and luminescence.[7] Especially luminescence is attracting an increasing attention as MOFs and coordination polymers enable beneficial effects bound to the hybrid character of these materials like antenna effects with metal to metal, ligand to metal energy transfers and vice versa as well as decreasing cross relaxation and thus the quenching of the luminescence by concentration of luminescence centers.[7c−e] The synthetic approach followed by our group involves the synthesis of new organic inorganic hybrid materials by solvent free melt reaction[8] of a metal with the melt of an organic, usually N-heterocyclic, linker molecule.[9−11] Part of the series of the 1,2,3-triazolates $^{3}_{\infty}[Ln(Tz^*)_3]$, namely, the heavier lanthanide homologues (Ln = Gd−Lu, Tz^{*-} = $C_2H_2N_3^-$, 1,2,3-triazolate anion, see Scheme 1) have already successfully been synthesized by this procedure together with 1*H*-1,2,3-triazole.[10] The mixed valent Eu triazolate $^{3}_{\infty}[Eu(Tz^*)_{6+x}(Tz^*H)_{2-x}]$[11] is known as well. However, the series of the light homologues La−Sm remain unknown. Network and framework structures of the lanthanides together with the other azolate rings like imidazolates show diverse and intense luminescence including 4f-4f and 5d-4f emission of lanthanide ions.[7d,e] Therefore, determination of the photoluminescence properties of lanthanide triazolates is interesting both with regard to elaborate this property previously unknown for these

Received: July 9, 2012
Published: November 21, 2012

Scheme 1. One Mesomeric Form of the 1,2,3-Triazolate Ligand

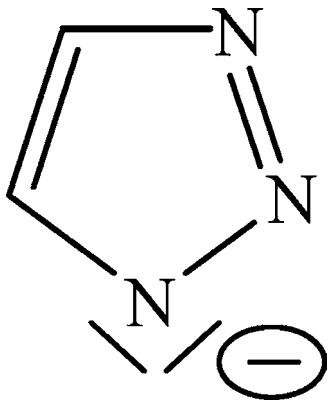

compounds and to compare it to other lanthanide azolates. Hence, we present the series of the lighter lanthanide triazolates $^{3}_{\infty}[Ln(Tz^*)_3]$, Ln = La, Ce, Nd, Pr, Sm (**1**–**5**), and take a close look at the photoluminescence behavior of the complete series of lanthanide 1,2,3-triazolates with Ln = La–Lu (**1**–**13**).

EXPERIMENTAL SECTION

General Procedures. All manipulations were carried out under inert atmospheric conditions using glovebox, ampule as well as vacuum line techniques. Reagents were successfully used without further purification (La (ChemPur, 99.9%), Ce (ChemPur, 99.9%), Pr (STREM, 99.9%), Nd (STREM, 99.9%), Sm (ChemPur, 99.9%), 1*H*-1,2,3-Triazole (ACROS, 97%).

For all reactions, to 0.5 mmol of the lanthanide metal and 1.8 mmol (slight excess regarding a stoichiometric reaction) of 1*H*-1,2,3-triazole, 10–20 mg of Hg were added for activation of the metals by amalgamation.[12] The reaction mixtures were frozen with liquid nitrogen and degassed three times. Because of the low melting point of 1,2,3-triazole around room temperature evacuation of the ampule containers enforces to freeze the mixture due to the vapor pressure of the ligand. As this is done with liquid nitrogen, Ar as inert atmosphere is also condensed. Therefore degassing and repetition is carried out. They were then sealed in DURAN glass ampules under vacuum. All reactions were carried out in Al_2O_3 tube ovens with EUROTHERM temperature control 2416 together with NiCr/Ni-temperature sensors. Purification of the products was carried out by evaporation and recondensation of excess ligand and mercury in sealed two-chamber ampules at temperatures between 100 and 120 °C. All reactions were carried out according to the procedure described above. Distinct reaction conditions and exceptions from the described method are listed below for each compound.

The IR spectra were recorded using a Bruker FTIR-IS66 V–S and a Thermo NICOLET 380 FT-IR spectrometer, the Raman spectra using a Bruker FRA 106-S spectrometer (1064 nm Nd:YAG-laser, 400 mW). For IR investigations KBr pellets were used under vacuum; investigation of Raman spectra used a 180° back scattering arrangement with a N_2 cooled Ge detector, the samples being prepared as fine powders in sealed thin glass tubes. Thermal Analysis was carried out on a NETZSCH STA 409 using alumina crucibles in a constant Ar/N_2-flow (50:50 ratio) of 20 mL/min at a constant heating rate of 10 K/min. Elemental analysis was carried out on a ELEMENTAR Vario El and ELEMENTAR Vario micro cube analyzer.

$^{3}_{\infty}[La(Tz^*)_3]$ (1). A 69 mg portion of La (0.5 mmol) and 104 mg of Tz* were treated as described above. The mixture was heated to 210 °C within 5 h, held at this temperature for 72 h, and then cooled to room temperature within 10 h. The reaction yielded 158 mg (91%) of a microcrystalline powder with light rose color. Anal. Calcd. $C_6H_6LaN_9$ (**1**): C, 21.01; N, 36.74; H, 1.76. Found: C, 21.2; N, 36.1; H, 1.9%. MIR (KBr): (3119 m, 2415 w, 1748 w, 1680 w, 1626 w, 1439 w, 1429 m, 1413 w, 1211 s, 1156 vs, 1085 vs, 985 s, 956 vs, 877 w, 825 s, 812 vs, 715 w) cm^{-1}. Raman: (1440 w, 1215 w, 1161 w, 156 w) cm^{-1}.

$^{3}_{\infty}[Ce(Tz^*)_3]$ (2). A 70 mg portion of Ce (0.5 mmol) and 104 mg of Tz* were treated accordingly to the procedure described above. The mixture was heated to 100 °C within 10 h and then to 160 °C within 20 h. The temperature was held for 500 h for annealing and then reduced to 80 °C within 27 h. After that, the ampule was cooled to room temperature within 6 h. The reaction yielded 168 mg (98%) of a colorless microcrystalline powder. Anal. Calcd. $C_6H_6CeN_9$ (**2**): C, 20.93; N, 36.61; H, 1.76. Found: C, 20.6; N, 36.0; H, 2.1%. MIR (KBr): (3119 m, 2417 w, 2174 w, 2120 w, 1748 w, 1680 w, 1626 w, 1439 w, 1428 m, 1412 w, 1213 s, 1158 vs, 1088 vs, 986 s, 956 vs, 878 w, 825 s, 809 vs, 715 m) cm^{-1}.

$^{3}_{\infty}[Pr(Tz^*)_3]$ (3). A 70 mg portion of Pr (0.5 mmol) and 104 mg of Tz* were treated as described above. The mixture was heated to 110 °C within 9 h and then to 170 °C within 20 h. The temperature was held for 500 h for annealing and then reduced to 90 °C within 27 h. Subsequently the ampule was cooled to room temperature within 7 h. The reaction yielded 144 mg (83%) of a light green microcrystalline powder. Anal. Calcd. C_6H_6 N_9Pr (**1**): C, 20.88; N, 36.53; H, 1.75. Found: C, 20.8; N, 36.0; H, 1.6%. MIR (KBr): (3120 m, 2499 vw, 2418 vw, 2299 vw, 2244 vw, 2179 vw, 1747 w, 1686 w, 1651 w, 1543 w, 1439 s, 1211 s, 1161 vs, 1092 vs, 987 s, 957 s, 879 w, 814 vs, 714 w) cm^{-1}. Raman: (1441 m, 1429 w, 1414 vw, 1215 m, 1165 m, 1095 w, 987 vw, 958 w, 160 m, 130 m) cm^{-1}.

$^{3}_{\infty}[Nd(Tz^*)_3]$ (4). A 72 mg portion of Nd (0.5 mmol) and 104 mg of Tz* were treated accordingly to the procedure described above. The mixture was heated to 150 °C within 6.5 h. The temperature was held for 50 h and then reduced to room temperature within another 6.5 h. The reaction yielded 155 mg (89%) of a colorless microcrystalline powder. Anal. Calcd. $C_6H_6N_9Nd$ (**4**): C, 20.68; N, 36.18; H, 1.74. Found: C, 21.0; N, 36.6; H, 2.3%. MIR (KBr): (3120 m, 2420 w, 1750 w, 1687 w, 1628 w, 1439 m, 1429 w, 1413 w, 1214 s, 1160 vs, 1099 s, 1092 vs, 988 s, 956 vs, 878 w, 826 m, 814 vs, 715 w, 431 w) cm^{-1}.

***β*-$^{3}_{\infty}[Sm(Tz^*)_3]$ (5).** A 75 mg portion of Sm (0.5 mmol) and 104 mg of Tz* were treated accordingly to the procedure described above. The mixture was heated to 167 °C within 164 h. The temperature was held for 191 h for annealing and then reduced to room temperature within 5 h. The reaction yielded 154 mg (87%) of a colorless microcrystalline powder. Anal. Calcd. $C_6H_6N_9Sm$ (**5**): C, 20.33; N, 35.56; H, 1.71. Found: C, 20.7; N, 35.2; H, 1.7%. MIR (KBr): (3155 w, 3120 s, 2648 vw, 2499 vw, 2420 w, 2299 vw, 2253 vw, 2187 vw, 1751 w, 1686 w, 1628 w, 1533 vw, 1439 vs, 1429 s, 1413 m, 1215 vs, 1165 vs, 1093 vs, 989 vs, 957 vs, 879 m, 816 vs, 715 m) cm^{-1}.

***α*-$^{2}_{\infty}[Sm(Tz^*)_3]$ (6).** A 75 mg portion of Sm (0.5 mmol) and 104 mg of Tz* were treated accordingly to the procedure described above. The mixture was heated to 130 °C within 3 h and to 155 °C within another 240 h. The temperature was held for 432 h for annealing and then reduced to room temperature within 8 h. The reaction yielded a limited number of colorless triangular shaped crystals in the area where the surface of the liquid ligand touches the walls of the ampule. Further reaction time for additional product formation as described for **5** results in vanishing of the single crystals of **6**. As only a few crystals are available no IR, Raman spectroscopy or microanalysis could be carried out.

$^{3}_{\infty}[Gd(Tz^*)_3]$ (7), $^{3}_{\infty}[Tb(Tz^*)_3]$ (8), $^{3}_{\infty}[Dy(Tz^*)_3]$ (9), $^{3}_{\infty}[Ho(Tz^*)_3]$ (10), $^{3}_{\infty}[Er(Tz^*)_3]$ (11), $^{3}_{\infty}[Yb(Tz^*)_3]$ (12), and $^{3}_{\infty}[Lu(Tz^*)_3]$ (13). These have been synthesized according to the procedures given in the original publication.[10]

Crystal Structure Determination. Powder patterns of **1**–**5** were recorded on STOE STADI P Debye–Scherrer X-ray diffractometers (Mo $K\alpha_1$ radiation λ = 0.70930 Å for compounds **1**–**4**, Cu $K\alpha_1$ radiation λ = 1.54059 Å for compound **5**; Ge-111 double monochromator, Debye–Scherrer geometry) at 297 K. The structures of the compounds have been refined with the Rietveld method and the program TOPAS,[13] using the fundamental parameters approach as reflection profiles (convolution of appropriate source emission profiles with axial instrument contributions as well as crystallite microstructure effects) and describing the preferred orientation of the crystallites with a spherical harmonics function of fourth order. The site parameters of

dx.doi.org/10.1021/ic301482e | *Inorg. Chem.* 2012, 51, 13204–13213

Table 1. Crystallographic Data for the Rietveld and Single Crystal Structure Refinements of 1−6

Formula	$C_6H_6N_9La$ (**1**)	$C_6H_6N_9Ce$ (**2**)	$C_6H_6N_9Pr$ (**3**)	$C_6H_6N_9Nd$ (**4**)	$C_6H_6N_9Sm$ (**5**)	$C_6H_6N_9Sm$ (**6**)	
Space group	*C*2/*c*					$R\bar{3}$	
Molar mass / $gmol^{-1}$	343.08	344.29	345.08	348.41	354.53	354.53	
a / pm	963.56(8)	958.84(6)	956.76(8)	955.16(8)	951.19(11)	863.86(4)	
b / pm	1668.43(12)	1661.50(10)	1655.07(11)	1649.29(12)	1637.2(14)		
c / pm	1316.39(11)	1307.81(9)	1300.86(10)	1295.37(12)	1286.83(13)	2380.7(2)	
β / °	94.166(6)	94.115(5)	93.981(6)	93.845(6)	93.659(7)		
Cell volume / nm^3	2.1107(3)	2.0781(2)	2.0598(3)	2.0361(3)	1.9999(3)	1538.6(2)	
Density / g/cm^3	2.1593(3)	2.2008(2)	2.2309(3)	2.2733(3)	2.3550(4)	2.296	
μ / cm^{-1}	44.220(6)	48.011(5)	51.876(7)	55.861(8)	443.46(8)	57.13	
Z	8					6	
Data collection	STOE STADI P					STOE IPDS I	
Radiation	Mo $K\alpha_1$, λ = 70.932 pm				Cu $K\alpha_1$, λ = 154.059 pm	Mo K_α, λ = 71.075 pm	
Reflections	710	1021	1149	1141	231	3636 overall, 1006 (unique)	
Data points	3101	3601	4000	3900	4900	Data range	2.85≤2θ≤30.31
d range	1.164	1.024	0.979	0.979	1.655		-12 ≤ h ≤ 12;
	–	–	–	–	–		-12 ≤ k ≤ 11;
	8.342	8.307	8.275	8.251	8.212		-33 ≤ l ≤ 17
Refined parameters	69	65	82	82	67	no. of parameters	57
(Background)	(24)	(24)	(36)	(36)	(36)	reflections / parameters	18
Wght. Durbin-Watson	1.260	1.317	1.376	0.426	1.816	R_1 [a] for n ref. with $F_o>4\sigma(F_o)$; n	0.031; 893
R_{bragg}	0.009	0.007	0.006	0.025	0.009	R_1 (all)	0.035
R_P	0.039	0.036	0.036	0.053	0.055	wR_2 [b] (all)	0.075
wR_P	0.050	0.046	0.046	0.069	0.070	remaining electron density	+ 1.28 /- 0.99 e/pm 10^6
χ^2	1.154	1.090	1.077	1.887	0.916		

the lanthanide ions were refined freely, refinement of the location of the 1,2,3-triazolate anions required the use of Z-matrices as rigid body constraints. Thus, position and orientation of each anionic ring were refined. Refinement of temperature factors was done isotropically except for compound **5**, where the low signal-to-noise ratio allowed no reasonable refinement of temperature factors. For the other compounds, the temperature factors of the lanthanide ions were refined freely. Refinement of the temperature factors of the C and N atoms could be achieved for compounds **3** and **4** using a constraint for both, C and N, atoms, refining one parameter for the temperature factor of each element. Temperature factors of H atoms were not refined. For compound **4**, a further constraint had to be implemented that excluded ring orientations that would result in unreasonably short Nd−N distances, again because of the low signal-to-noise ratio.

For investigation of the crystal structure of **6**, a suitable single crystal was selected and sealed in a glass capillary under glovebox conditions. The data collection was carried out on a STOE IPDS-I diffractometer (Mo K_α radiation λ = 0.7107 Å) at 140 K. The structure was determined using direct methods.[16] All non-H atoms were refined anisotropically by least-squares techniques.[17] The hydrogen atom positions were also deduced from the electron density card and refined isotropically. $^2_\infty[Sm(Tz^*)_3]$ crystallizes isotypic to $^2_\infty[Tb(Tz^*)_3]$ (α-phase)[18] in the rhombohedral space group $R\bar{3}$. For all compounds, the space group selection was separately checked for higher or other symmetry.[19] Crystallographic data for compounds **1**−**6** are summarized in Table 1.

Further information was deposited at the Cambridge Crystallographic Data Centre, CCDC, 12 Union Road, Cambridge CB2 1EZ, U.K. (fax: +44 1223336033 or e-mail: deposit@ccdc.cam.ac.uk) and may be requested by citing the deposition numbers CCDC-883820 (**1**), 883821 (**2**), 883822 (**3**), 883823 (**4**), 883824 (**5**), 883825 (**6**), the name of the authors and the literature citation.

Photoluminescence Spectroscopy. Excitation and emission spectra were recorded with a Jobin Yvon Horiba Fluorolog 3 equipped with a 450 W Xe-lamp, an integrating sphere as well as double integrating excitation and emission monochromators. Excitation spectra have been corrected from 250 to 600 nm for the spectral distribution of the lamp intensity using a photodiode reference detector. Emission spectra were also corrected for the spectral response of the monochromators and the detector using typical correction spectra provided by the manufacturer. To avoid first order scattering effects spectral contributions below 400 nm were filtered by

dx.doi.org/10.1021/ic301482e | Inorg. Chem. 2012, 51, 13204−13213

the use of edge filters (400GG Reichmann-Optik). Measurement parameters can be found in the Supporting Information. Emission spectra for the calculation of color points have been recorded at the highest excitation wavelength possible, to avoid the necessity of the use of edge filters that could have a falsifying effect on the calculation, especially for compounds with an emission maximum located in the area below 450 nm, and significant spectral contributions are present below 400 nm.

RESULTS AND DISCUSSION

Crystal Structure. The results of the Rietveld refinements show, that compounds **1**−**5** crystallize isotypic to the dense MOF $^{3}_{\infty}[Tb(Tz^*)_3]$ (β-phase)[10] in the monoclinic space group $C2/c$. They are formed according to stoichiometric reactions of the metals with 1*H*-1,2,3-triazole.

Scheme 2. . Equation for the Reaction of a Lanthanide Metal (Ln) with 1*H*-1,2,3-Triazole (Tz*H)

$$Ln + 3\ Tz^*H \xrightarrow[Hg\ (cat)]{\Delta} {}^{3}_{\infty}[Ln(Tz^*)_3] + {}^{3}/_{2}\ H_2$$

As an example for the results of the Rietveld refinements, the experimental and calculated powder patterns of **2** are shown in Figure 1, and the other Rietveld plots are listed in the Supporting Information.

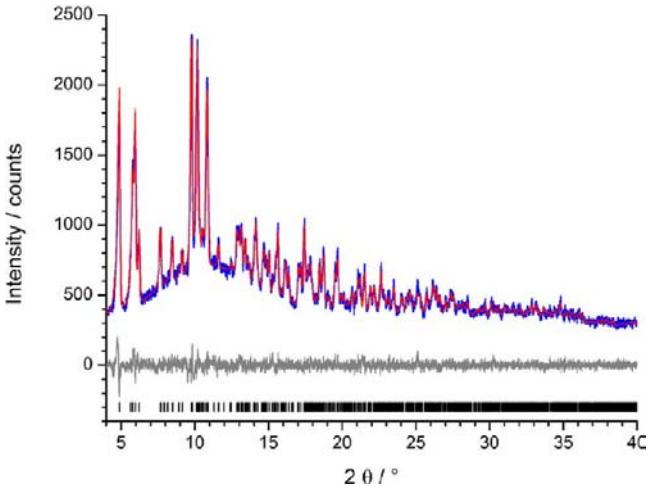

Figure 1. Graph for the Rietveld refinement of $^{3}_{\infty}[Ce(Tz^*)_3]$ (**2**). The observed diffractogram is plotted in blue, and the refined in red. The difference plot is displayed in dark gray; black tick marks indicate Bragg reflection conditions.

Low concentrations of side phases are present in samples of **1**, **3**, and **4** as well. According to the powder diffraction data, they justify refinement as different lanthanide hydrides. The presence of lanthanide hydrides as minor impurities is not uncommon in systems that originate from the use of lanthanide metals, as reaction with hydrogen, which is formed during the reaction by deprotonation of the organic ligand (see Scheme 1), occurs already at room temperature.[14,15] Moreover, it is known that lanthanide hydrides are a possible impurity in commercially available lanthanide metals, or can easily be formed by contamination of the reaction samples with traces of moisture.[14]

Like the heavier lanthanide-1,2,3-triazolates,[10] **1**−**5** exhibit the β-$^{3}_{\infty}[Ln(Tz^*)_3]$ structure (see Figure 2), a three-dimensional (3D) framework structure that is built of octahedra

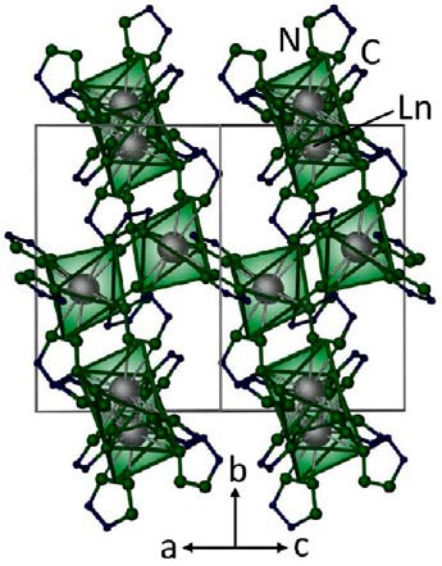

Figure 2. Crystal structure of $^{3}_{\infty}[Ln(Tz^*)_3]$. View along [110], lanthanide atoms are displayed in gray, carbon atoms in blue, and nitrogen atoms in green. H atoms are omitted for clarity, edges of the polyhedra do not represent bonds.

formed by the centers of the six 1,2,3-triazolate anions surrounding each lanthanide cation. Each of these octahedra connects to three further octahedra via non-adjacent edges, resulting in a complex (10,3) net that can be derived from a Wells's (10,3)-b net, which can, for example, be found in phosphorus pentoxide P_4O_{10}.[20] The lanthanide contraction from La to Sm is fulfilled as the Ln−N distances of **1**−**5** reflect the decrease in the atomic radii.[21] Suitable restraints have been implemented in the refinement when necessary. This step is essential, as refinements from powder data cannot deliver results that match the precision and reliability of single crystal data. Bond length discussion shall thus be limited to the refinements that are free of atom distance restraints. The La−N distances in **1** reach from 235(3) pm to 277(4) pm and are in the range of La−N distances known from other coordination compounds, for example, La[CyNC(SiMe$_3$)NCy]-(N(SiMe$_3$)$_2$)$_2$ (237.7−248.6 pm),[22a] [{(*i*PrN)$_2$C[NLi(THF)$_3$(C$_6$H$_9$*p*-Cl)]}$_2$La(μ-Cl$_2$)Li(THF)$_2$]·2THF (245.3−251.4 pm)[22b] or [LaCl$_2$(Tp^{Me2})(bipy)] (260.0−269.9 pm).[22c] $^{3}_{\infty}[La(Btz)_3]$ (Btz$^-$ = benzotriazolate anion, $C_6H_4N_3^-$), where the La^{3+}-cation is also surrounded by an octahedral coordination sphere built of nine nitrogen atoms via η^1- and η^2-coordination modes, shows La−N distances from 251 to 296 pm.[22d] For **2**, Ce−N distances of 237(3) to 270(3) pm were observed which are in good accordance with other coordination polymers that exhibit Ce−N distances like 251.4 pm in $\{[Ce_2(Hpimda)_2(\mu_4\text{-}C_2O_4)\cdot 2H_2O\}_n$[23a] or 261.8−278.5 pm in $\{[Ce_2(bpm)(dmf)_8(H_2O)_2]\text{-}[W(CN)_8]_2\}_n$.[23b] The dimeric cerium complex [Ce$_2$(Dpa)$_6$] shows Ce−N distances that reach from 241 to 273 pm,[23c] which is approximately the same range of atomic distances like in **2**. The refinements of the structures of **3**−**5** do not justify bond length discussion as they involved the use of restraints regarding the Ln−N distances, which makes a discussion of these parameters futile.

In contrast to **1**−**5**, **6** crystallizes isotypic to the already known α-$^{2}_{\infty}[Tb(Tz^*)_3]$, which adopts the AlCl$_3$-structure type, a 2D layer structure (see Figure 3).[18] This structure is also built by octahedra of the centers of the 1,2,3-triazolate anions

dx.doi.org/10.1021/ic301482e | *Inorg. Chem.* 2012, 51, 13204−13213

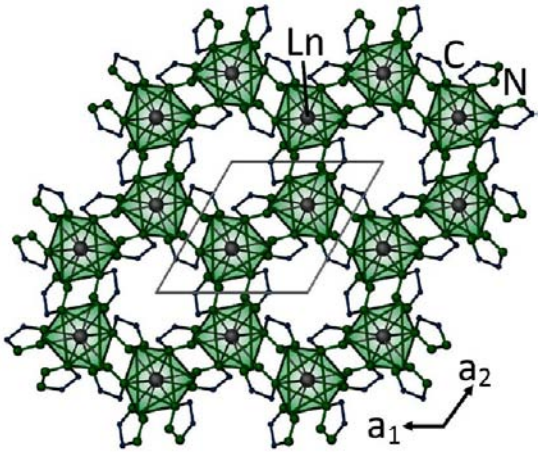

Figure 3. View along [001] on one layer of the crystal structure of α-$^{2}_{\infty}$[Sm(Tz*)$_3$]. Sm atoms are displayed in gray, N atoms in green, and C atoms in blue. H atoms are omitted for clarity. Edges of the polyhedra do not represent bonds.

surrounding the Sm atoms. The Sm−N distances reach from 240.7(3) to 261.1(4) pm and agree with those observed in other Sm^{III}-amides such as {{[−(CH$_2$)$_5$−]$_4$-Calix-tetrapyrrole}-Sm^{III}}$_2$(μ-C$_2$Li$_4$)·Et$_2$O with 237.1−266.0 pm.[23d] They are slightly longer than the Tb−N distances observed in the isostructural α-$^{2}_{\infty}$[Tb(Tz*)$_3$], which reach from 236.3 to 259.7 pm. This is in good accordance with the expected decrease in the Ln−N distances originating from the decrease of the atomic radii from Sm^{3+} to Tb^{3+}[21] because of the lanthanide contraction.

Photoluminescence Properties. The photoluminescence properties of **2**−**5** and of the MOFs $^{3}_{\infty}$[Gd(Tz*)$_3$] (**7**), $^{3}_{\infty}$[Tb(Tz*)$_3$] (**8**), $^{3}_{\infty}$[Dy(Tz*)$_3$] (**9**), $^{3}_{\infty}$[Ho(Tz*)$_3$] (**10**), $^{3}_{\infty}$[Er(Tz*)$_3$] (**11**), $^{3}_{\infty}$[Yb(Tz*)$_3$] (**12**), and $^{3}_{\infty}$[Lu(Tz*)$_3$] (**13**) were investigated regarding excitation and emission (see Figures 4, 5, and 6) and color points. Distinct wavelengths for measuring the excitation and emission spectra, as well as the respective color points of the emission, are listed in Table 2.

The spectral properties of the anionic ligand bound within the structures of the isotypic frameworks could be derived from the photoluminescence measurements of **7**, as the energy levels of the Gd^{3+}-ion are located in the area above 32000 cm^{-1} and thus would only affect excitation and emission within the UV region of the spectrum. In the excitation spectrum of **7**, we observe a distinct maximum at 360 nm, as well as two shoulders at 285 and 310 nm that by comparison with the excitation and emission spectra of the free ligand (see Supporting Information) can be identified with the q-bands of the ligand in addition to the p-bands below 280 nm. The emission spectrum shows a very broad signal, covering almost the complete wavelength range investigated, with its maximum at 521 nm and a broad shoulder at around 460 nm. This emission can be assigned to a $T_1 \rightarrow S_0$ transition of the triazolate anions. $^{3}_{\infty}$[Pr(Tz*)$_3$] (**3**), $^{3}_{\infty}$[Nd(Tz*)$_3$] (**4**), $^{3}_{\infty}$[Sm(Tz*)$_3$] (**5**), $^{3}_{\infty}$[Ho(Tz*)$_3$] (**10**), $^{3}_{\infty}$[Er(Tz*)$_3$] (**11**), and $^{3}_{\infty}$[Lu(Tz*)$_3$] (**13**) show qualitatively rather similar excitation and emission spectra. They all show broad excitation bands with their highest maxima below 280 nm, a more or less distinct maximum around 360 nm, and the shoulders at 285 and 310 nm that can be again assigned to the p- and q-bands of the triazolate ligand. The emission spectra also show very broad signals that are identified with $T_1 \rightarrow S_0$ transitions of the triazolate anions.

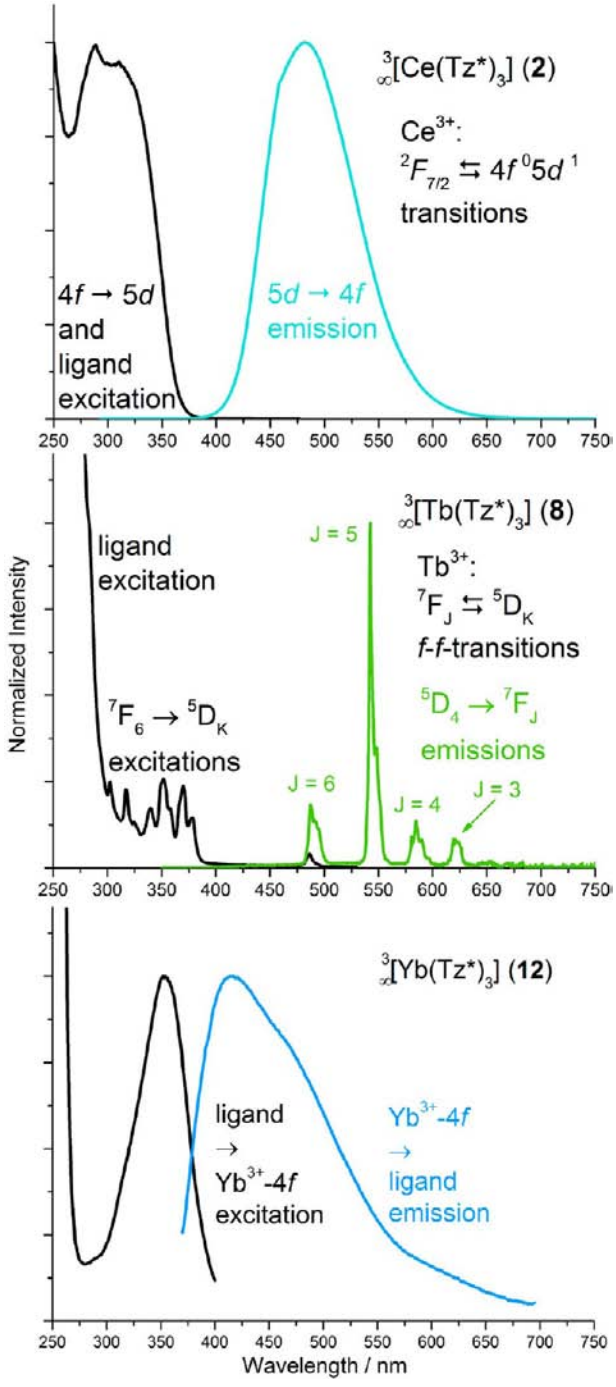

Figure 4. Excitation and emission spectra of the lanthanide triazolates **2** (Ce), **8** (Tb), and **12** (Yb) showing 4f-5d- (**2**), 4f-4f- (**8**), and CT-transitions (**12**).

However profiles and maxima differ from the gadolinium containing dense MOF **7**. The maxima are found between 426 (**4**) and 585 nm (**11**) and are responsible for a shift in the color points of the organic fluorescence (see Figure 7).

The emission spectra of **3**, **4**, **5**, **10**, and **11** show indications for the participation of the Ln^{3+} ions. While the emission curves of **7** and **13** are both smooth curves, the signals of the compounds mentioned show indentations, just like an absorption spectrum atop the emission signal. We attribute this to an inner filter effect of the lanthanide ions, as these indentations can be assigned to excitations to various energy

dx.doi.org/10.1021/ic301482e | Inorg. Chem. 2012, 51, 13204−13213

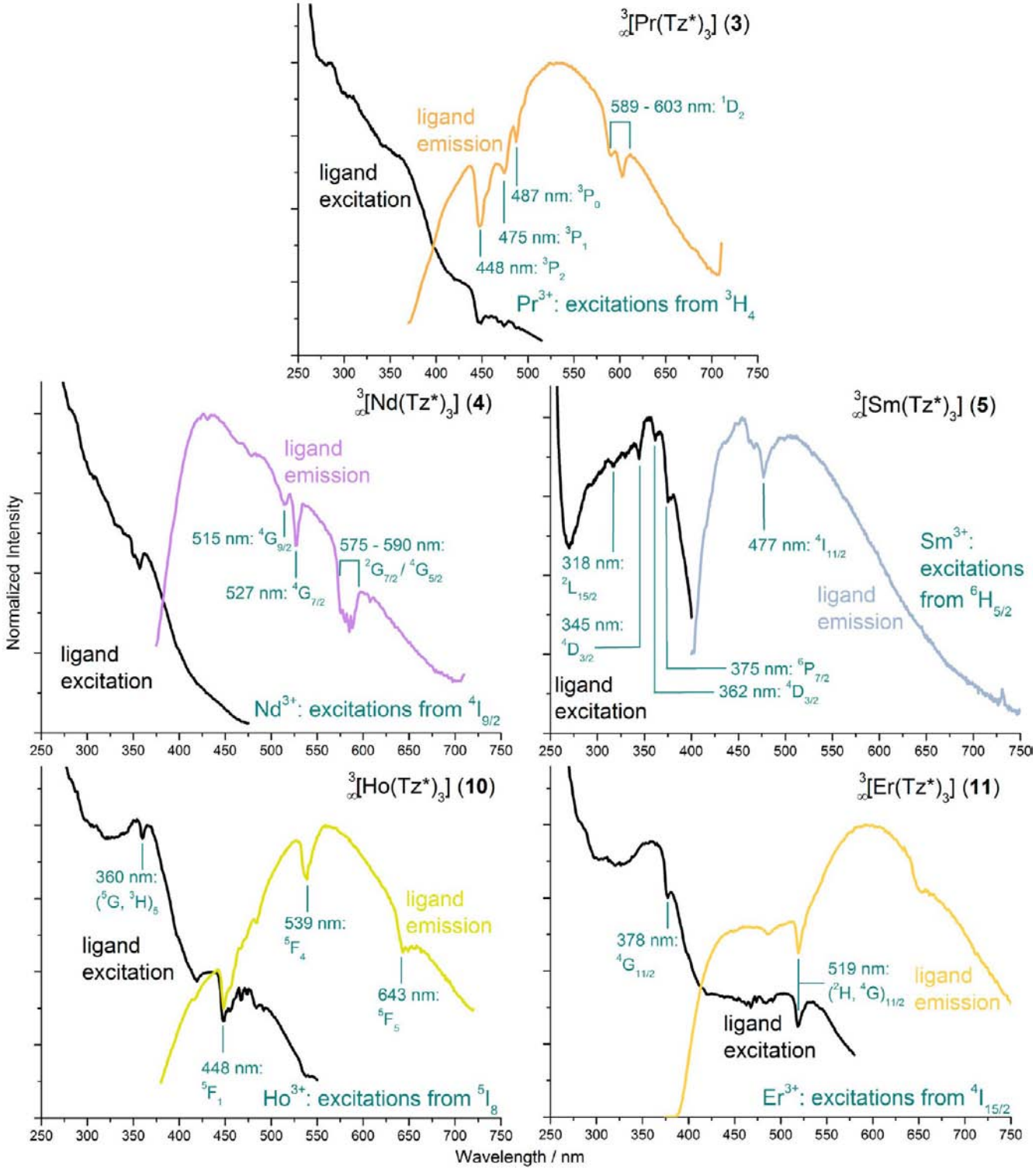

Figure 5. Excitation and emission spectra of the lanthanide triazolates **3** (Pr), **4** (Nd), **5** (Sm), **10** (Ho), and **11** (Er). Green labels indicate reabsorption of emitted ligand radiation by Ln^{3+} ions, causing an inner-filter effect.

levels of the Ln^{3+} ions and thus indicate reabsorption of the light emitted from the organic ligand by the Ln^{3+} ions.[24] Whereas the inner filter effect was initially observed in pyrene fluorescence spectra after mixing pyrene with sodium oxidiacetato-holmate(III),[24a] we observe this effect in the triazolate ligand emission peak of the compound containg the lanthanide ions. To the best of our knowledge, this is the first example of such a type of inner-filter effect. Wavelengths and possible corresponding energy levels concerning this phenomenon are displayed for each compound within Figures 4, 5, and 6.

The spectra of $^3_\infty$[Dy(Tz*)$_3$] (**9**) show a different lanthanide participation. The excitation spectrum shows additional intensities at 325, 315, and 365 nm on a curve that otherwise resembles the excitation spectra of the already mentioned compounds. These wavelengths match several excitations from

dx.doi.org/10.1021/ic301482e | *Inorg. Chem.* 2012, 51, 13204−13213

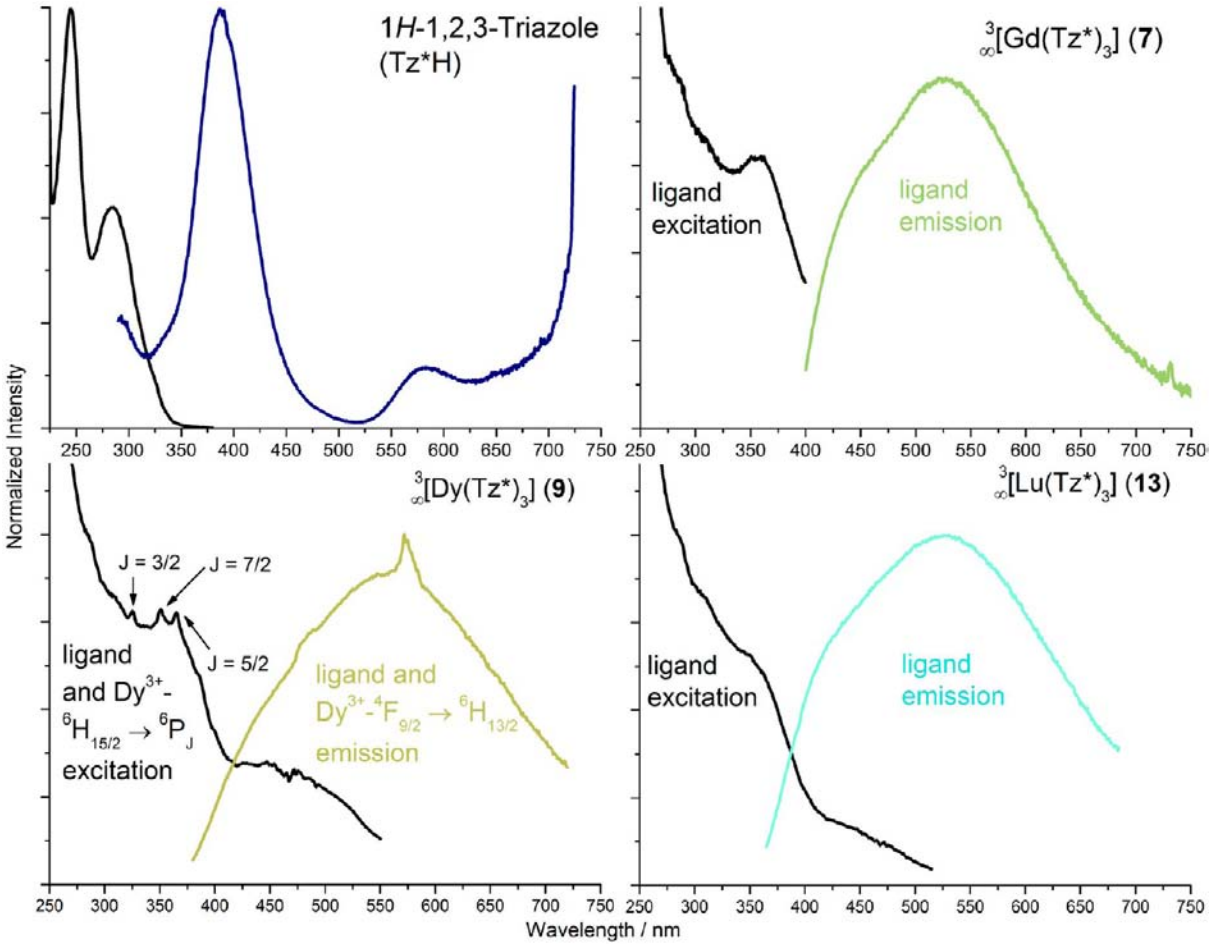

Figure 6. Excitation and emission spectra of the ligand 1*H*-1,2,3-triazole and the remaining lanthanide triazolates **7** (Gd), **9** (Dy), and **13** (Lu).

Table 2. Investigation of the Photoluminescence Properties of the Lanthanide Triazolates 2−12

	excitation spectrum		emission spectrum		
compound	λ_{Em}	λ_{max} [a]	λ_{Ex}	λ_{max} [b]	color point
$^3_\infty$[Ce(Tz*)$_3$] (**2**)	487	288/312	288	488	x = 0.159; y = 0.287
$^3_\infty$[Pr(Tz*)$_3$] (**3**)	530	285/310/360	360	531	x = 0.365; y = 0.383
$^3_\infty$[Nd(Tz*)$_3$] (**4**)	486	285/310/360	362	426	x = 0.290; y = 0.288
β-$^3_\infty$[Nd(Tz*)$_3$] (**5**)	455	355	365	454	x = 0.277; y = 0.323
$^3_\infty$[Gd(Tz*)$_3$] (**7**)	528	285/310/360	365	521	x = 0.307; y = 0.372
$^3_\infty$[Tb(Tz*)$_3$] (**8**)	543	283/303−378	283	487/**543**/584/620	x = 0.327; y = 0.558
$^3_\infty$[Dy(Tz*)$_3$] (**9**)	574	285/310/325/351/365	365	560/**572**	x = 0.355; y = 0.389
$^3_\infty$[Ho(Tz*)$_3$] (**10**)	560	285/310/350/365	365	562	x = 0.360; y = 0.401
$^3_\infty$[Er(Tz*)$_3$] (**11**)	600	285/310/360	285	585	x = 0.389; y = 0.397
$^3_\infty$[Yb(Tz*)$_3$] (**12**)	412	354	354	417	x = 0.204; y = 0.209
$^3_\infty$[Lu(Tz*)$_3$] (**13**)	530	285/310/350	350	525	x = 0.315; y = 0.357

[a]Local maxima above 250 nm. [b]bold = main maxima.

the $^6H_{15/2}$ ground state to higher energy levels of the Dy^{3+}-ion.[25] The emission spectrum shows a broad band with a very distinct and sharp additional band at 572 nm that can be identified with the $^4F_{9/2} \rightarrow {}^6H_{13/2}$ transition in the Dy^{3+}-ion, as well as a signal atop the curve at 480 nm that belongs to the $^4F_{9/2} \rightarrow {}^6H_{15/2}$ transition. These additional signals in the emission spectrum can be observed regardless of the excitation wavelength. Thus, the occurrence of an antenna effect by a ligand to metal energy transfer in the luminescence of $^3_\infty$[Dy(Tz*)$_3$] can be stated. However, the emission of the organic part of the hybrid material strongly dominates the overall emission.

The spectra of $^3_\infty$[Yb(Tz*)$_3$] (**12**) show a lesser bandwidth than the compounds described before. In addition to the p-band below 280 nm the excitation spectrum shows a more pronounced q-band signal from 285 to 400 nm with a maximum at 354 nm. The emission spectrum shows a band starting at 370 nm with a maximum at 417 nm and a shoulder

dx.doi.org/10.1021/ic301482e | *Inorg. Chem.* 2012, 51, 13204−13213

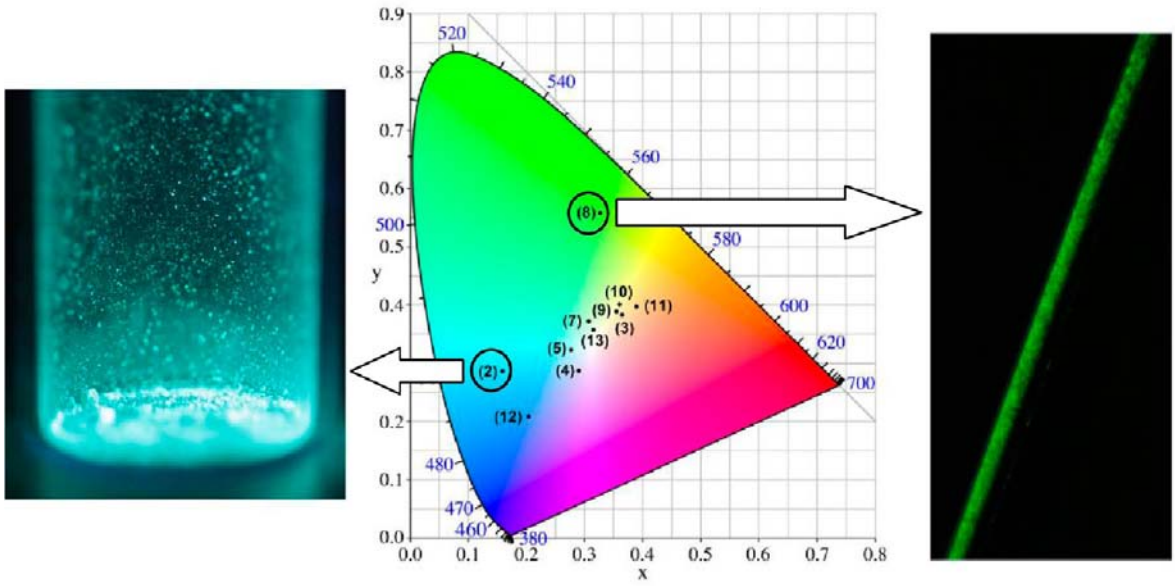

Figure 7. Color points and color diagram (CIE[35]) of the emissions of the investigated lanthanide 1,2,3-triazolates (middle) and images depicting the luminescence phenomena of $^3_\infty[Ce(Tz^*)_3]$ (**2**, left) and $^3_\infty[Tb(Tz^*)_3]$ (**8**, right).

around 470 nm that reaches up to around 550 nm. Both signals cannot be identified with Yb^{3+}-f-f-transitions, but are assigned to charge transfer (CT) transitions between the ligand and 4f states of the Yb^{3+} ion. Compounds like $Y_2O_2S:Yb^{3+}$, $La_2O_2S:Yb^{3+}$,[26] or $KLa_{1-x}Yb_x(PO_3)_4$ (x = 5−20%)[27] show excitation and emission spectra with maxima at 270 to 310 nm for excitation and 300 to 430 nm for emission. The CT process depends on a number of parameters such as temperature and electron affinity of the ligand,[26] which result in a broad range in which the energy transfers can occur, depending on the specific system that is investigated. Under these circumstances, the excitation and emission maxima observed for **12** are in good accordance with the examples found in literature. Thus, the interpretation of the photoluminescence behavior of $^3_\infty[Yb(Tz^*)_3]$ as being based on Yb^{3+} CT transitions seems legitimate.

The luminescence of $^3_\infty[Ce(Tz^*)_3]$ (**2**) is by far the most intense observed for the compounds presented here and can be described as a light blue emission (see Figure 4 and 7). It is based on a broad emission signal from 415 to 600 nm with an emission maximum at 482 nm. Excitation shows two maxima, a smaller one at 288 nm and the higher at 312 nm. The photoluminescence behavior of this compound is in good accordance with other luminescent Ce^{3+} containing compounds, like $Lu_2CaMg_2(Si,Ge)_3O_{12}:Ce^{3+}$ or the system $Y_{1.98}Ce_{0.02}Si_{3-x}Al_xO_{3+x}N_{4-x}$,[28] especially MOFs that also emit in the blue region like $^3_\infty[Ce(Im)_3(ImH)]\cdot ImH$ or $^2_\infty[Sr(Im)_2(ImH)_2]:Ce$.[9a] Thus in comparison with the other azolates 1,2,3-triazolate and imidazolate show equal behavior. Ce^{3+} is the only trivalent lanthanide ion which exhibits reduction of the energy of 5d states by splitting of the crystal and ligand fields that enables 4f → 5d excitation within the UV region close to the visible and 5d → 4f emission in the visible region of the spectrum.[29] Inclusion of 5d states is also responsible for broad band transitions as the ground and excited states involved differ position dependent between close core and valence electrons. Excitation of 5d states also results in dependence on the chemical surrounding, which in the case of the cerium 1,2,3-triazolate **2** leads to a blue emission alike $^3_\infty[Ce(Im)_3(ImH)]\cdot ImH$ or $^2_\infty[Sr(Im)_2(ImH)_2]:Ce$ and different from the yellow emission of a Ce-YAG laser.[30] Disappearance of the organic emission band in favor of the 5d → 4f emission of cerium points out that an effective ligand to metal energy transfer is observed and thus a strong antenna effect is present for $^3_\infty[Ce(Tz^*)_3]$ (**2**).

The photoluminescence spectra of $^3_\infty[Tb(Tz^*)_3]$ (**8**) indicate typical Tb^{3+} luminescence[31] as well as an antenna effect of the organic ligand. The excitation spectrum recorded from 280 to 530 nm shows a broad excitation band from 250 to 300 nm, originating from q-band of the organic ligand as well as a shoulder at 283 nm, several sharp signals between 300 and 385 nm, and another sharp signal at 487 nm. All sharp excitation signals can be assigned to direct Tb^{3+} excitation.[31] The excitation maxima at 303, 317, 325, 340, and 352 nm can be identified with $^7F_6 \rightarrow {}^5D_2$ transitions, the signals at 358, 370, and 379 nm belong to $^7F_6 \rightarrow {}^5D_3$ excitations, the signal at 488 nm originates from a $^7F_6 \rightarrow {}^5D_4$ transition. Emission of the compound shows the typical f−f based $^5D_4 \rightarrow {}^7F_J$ transitions (J = 6−3) at 488, 543, 585, and 619 nm as sharp signals, with the $^5D_4 \rightarrow {}^7F_5$ emission at 543 nm as the emission maximum. The $^5D_4 \rightarrow {}^7F_J$ transitions with J = 2−0 around 650, 667, and 680 nm are present but very weak in intensity. While excitation was done at 283 nm, within the excitation band of the organic ligand, the emission spectrum only shows Tb^{3+} emission and no detectable emission of the organic ligand, thus confirming an efficient antenna effect for the luminescence of $^3_\infty[Tb(Tz^*)_3]$. A depiction of the green luminescence of the compound can be found in Figure 7.

The photoluminescence spectra of $^3_\infty[La(Tz^*)_3]$ and $^3_\infty[Lu(Tz^*)_3]$ are not discussed in detail. While the lanthanum compound is contaminated with traces of Ce^{3+}, that dominate the emission and excitation behavior of the compound, $^3_\infty[Lu(Tz^*)_3]$ shows rather large amounts of nonvolatile decomposition products of the organic ligand, because of its higher formation temperature compared to the other compounds, that falsify further analytic investigation besides powder diffraction and include the quenching of any luminescence phenomena.

dx.doi.org/10.1021/ic301482e | *Inorg. Chem.* 2012, 51, 13204−13213

Altogether, the luminescence of lanthanide triazolates is various, covering a broad range of the rare earth ions and corroborates other azolates like lanthanide imidazolates. It strongly depends on the specific lanthanide ion, if 4f-4f emission, 4f-5d, or CT transitions or organic fluorescence are observed, with the 1,2,3-triazolate ion being a suitable antenna for a ligand to metal energy transfer.

Thermal Properties. As examples, the thermal properties of **1**, **3**, and **5** were investigated using simultaneous differential thermal analysis-thermogravimetry (DTA/TG) experiments from 20 to 800 °C. All three compounds exhibit only one strong sharp exothermic signal at 350 °C (**1**), 365 °C (**3**), and 360 °C (**5**), respectively (see Figure 8), accompanied by a loss of 27−30% of the sample mass, indicating decomposition of the framework structures. The release of triazole molecules is improbable because of the homoleptic character of the frameworks, in which all ligands are formal anions with no neutral triazole molecules being present. The exothermic step in the DTA signal instead implies the formation of N_2 as stable product of the decomposition of the triazolate anions. This is in good agreement with the thermal properties of the recently investigated heavier lanthanide 1,2,3-triazolates,[10] which also show only one sharp exothermic signal due to N_2 release in the DTA/TG investigations.

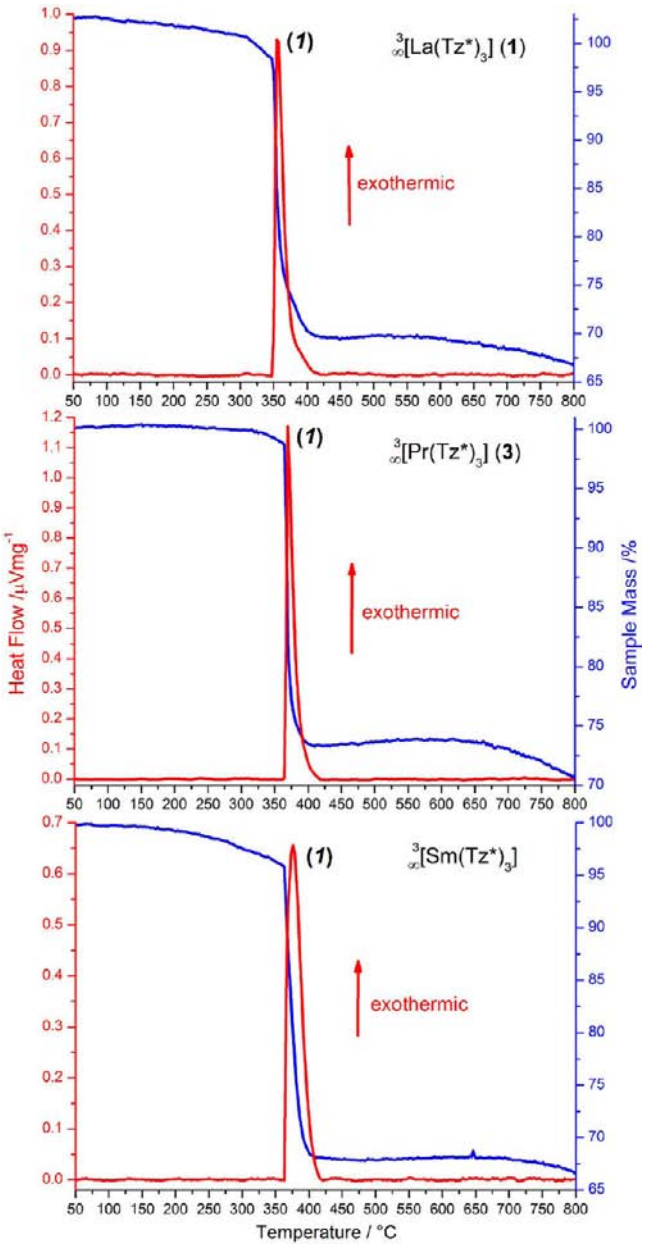

Figure 8. Investigation of the thermal behavior of **1**, **3**, and **5** (from top to bottom) by simultaneous DTA/TG (heating rate 10 K/min). The heat flow is plotted in red, and the mass course in blue.

Vibrational Analysis. Raman spectra of satisfying quality could be obtained for **1** and **3**. The Raman bands in the area from 1440 to 970 are associated with stretching and in-plane-bending vibrational modes[32] and confirm the presence of the triazolate anion (see Supporting Information). Additional bands observed in the range of 160 cm^{-1} can be identified with lattice vibrations.[33] Compared to the spectrum of the free ligand,[34] the IR spectra of **1**−**5** show splitting as well as small shifts for several bands, indicating binding to the lanthanide cations. The purity of the samples and the homoleptic character of the network are confirmed by the absence of the ν(NH) stretching mode at 3357 cm^{-1}.

CONCLUSIONS

The series of lanthanides La−Lu yield two-dimensional and 3D networks from reactions with molten 1*H*-1,2,3-triazole, with the exception of Eu because of mixed valence of the latter. All other lanthanides give homoleptic trivalent 1,2,3-triazolate compounds. This series of dense MOFs $^3_\infty$[Ln(Tz*)$_3$] (Tz*$^-$ = 1,2,3-triazolate anion, $C_2H_2N_3^-$) shows an exceptional variety of photoluminescence properties as six different luminescence phenomena are found for one crystal structure: Depending on the lanthanide ion they show ligand based fluorescence, f-f or f-d emission, and CT based photoluminescence properties, as well as ligand based antenna effects of varying efficiency. In addition, inner-filter effects are found in the ligand emission bands that are attributed to reabsorption of the emitted light by the trivalent lanthanide ions. Therefore the series of dense frameworks qualify as hybrid materials with remarkable photoluminescence properties. To the best of our knowledge, this is the first example that such a diversity of effects has been observed for one series of coordination polymers and frameworks, especially in combination with the homoleptic character of the compounds presented here.

ASSOCIATED CONTENT

Supporting Information

Further details are given in 16 figures, 1 table, additional Rietveld plots, photoluminescence spectra, experimental measurement details for photoluminescence spectroscopy, Raman spectra, CIF files. This material is available free of charge via the Internet at http://pubs.acs.org.

AUTHOR INFORMATION

Corresponding Author

*Phone: +49 931 31-88724. Fax: +49 931 31-84785. E-mail: klaus.mueller-buschbaum@uni-wuerzburg.de.

Author Contributions

The manuscript was written through contributions of all authors. All authors have given approval to the final version of the manuscript.

Notes

The authors declare no competing financial interest.

■ ACKNOWLEDGMENTS

We thank the Deutsche Forschungsgemeinschaft (DFG project MU-1562/4-2), the University of Würzburg as well as the Wilhelm-Klemm foundation for supporting this work.

■ REFERENCES

(1) Stock, N.; Biswas, S. *Chem. Rev.* **2012**, *112*, 933−969.
(2) (a) Tan, C.; Yang, S.; Champness, N. R.; Lin, X.; Blake, A. J.; Lewis, W.; Schröder, M. *Chem. Commun.* **2011**, *47*, 4487−4489. (b) Murray, L. J.; Dincă, M.; Long, J. R. *Chem. Soc. Rev.* **2009**, *38*, 1294−1314.
(3) (a) Li, J.-R.; Ma, Y.; McCarthy, M. C.; Sculley, J.; Yu, J.; Jeong, H.-K.; Balbuena, P. B.; Zhou, H.-C. *Coord. Chem. Rev.* **2011**, *255*, 1791−1823. (b) Li, J.-R.; Kuppler, R. J.; Zhou, H.-C. *Chem. Soc. Rev.* **2009**, *38*, 1477−1504.
(4) Cheetham, A. K.; Rao, C. N. R. *Science* **2007**, *318*, 58−59.
(5) (a) Dey, C.; Das, R.; Saha, B. K.; Poddar, P.; Banerjee, R. *Chem. Commun.* **2011**, *47*, 11008−11010. (b) Kurmoo, M. *Chem. Soc. Rev.* **2009**, *38*, 1353−1379.
(6) (a) Allendorf, M. D.; Schwartzberg, A.; Stavila, V.; Talin, A. A. *Chem.—Eur. J.* **2011**, *17*, 11372−11388. (b) Alvaro, M.; Carbonell, E.; Ferrer, B.; Labrés i Xamena, F. X.; Garcia, H. *Chem.—Eur. J.* **2007**, *13*, 5106−5112.
(7) (a) Guo, J.; Ma, J.-F.; Liu, B.; Kan, W.-Q.; Yang, J. *Cryst. Growth Des.* **2011**, *11*, 3609−3621. (b) Höller, C. J.; Mai, M.; Feldmann, C.; Müller-Buschbaum, K. *Dalton Trans.* **2010**, *39*, 461−468. (c) Allendorf, M. D.; Bauer, C. A.; Bhakta, R. K.; Houk, R. J. T. *Chem. Soc. Rev.* **2009**, *39*, 1330−1352. (d) Zurawski, A.; Mai, M.; Baumann, D.; Feldmann, C.; Müller-Buschbaum, K. *Chem. Commun.* **2011**, *47*, 496−498. (e) Müller-Buschbaum, K.; Torres, S. G.; Larsen, P.; Wickleder, C. *Chem. Mater.* **2007**, *19*, 655−659.
(8) Müller-Buschbaum, K. *Z. Anorg. Allg. Chem.* **2005**, *631*, 811−828.
(9) (a) Zurawski, A.; Rybak, J.-C.; Meyer, L. V.; Matthes, P. R.; Stepanenko, V.; Dannenbauer, N.; Würthner, F.; Müller-Buschbaum, K. *Dalton Trans.* **2012**, *41*, 4067−4078. (b) Müller-Buschbaum, K.; Schönfeld, F. *Z. Anorg. Allg. Chem.* **2011**, *637*, 955−960. (c) Höller, C. J.; Müller-Buschbaum, K. *Eur. J. Inorg. Chem.* **2010**, 454−460.
(10) Rybak, J.-C.; Tegel, M.; Johrendt, D.; Müller-Buschbaum, K. *Z. Kristallogr.* **2010**, *225*, 187−194.
(11) Müller-Buschbaum, K.; Mokaddem, Y. *Solid State Sci.* **2008**, 416−420.
(12) Magyar, B. *Inorg. Chem.* **1968**, *7*, 1457−1458.
(13) Coelho, A. *TOPAS-Academic*, Version 4.1; Coelho Software: Brisbane, Australia, 2007.
(14) Simon, A. *Angew. Chem.* **2012**, *124* (18), 4354−4361.
(15) (a) Korst, W. L.; Warf, J. C. *Inorg. Chem.* **1966**, *5* (10), 1719−1726. (b) Mulford, R. N. R.; Holley, C. E. *J. Phys. Chem.* **1955**, *59* (12), 1222−1226.
(16) Sheldrick, G. M. *SHELXS-97, Program for the resolution of Crystal Structures*; University of Göttingen: Göttingen, Germany, 1997.
(17) Sheldrick, G. M. *SHELXL-97, Program for the refinement of Crystal Structures*; University of Göttingen: Göttingen, Germany, 1997.
(18) Rybak, J.-C.; Müller-Buschbaum, K. *Z. Anorg. Allg. Chem.* **2009**, *635*, 1134−1138.
(19) Spek, A. L. *PLATON-2000, A Multipurpose Crystallographic Tool*, V1.07; University of Utrecht: Utrecht, The Netherlands, 2003.
(20) Wells, A. F. *Three-dimensional nets and polyhedral*; Wiley-Inter-Science: New York, 1977.
(21) Shannon, R. D. *Acta Crystallogr., Sect. A* **1976**, *32*, 751−767.
(22) (a) Giesbrecht, G. R.; Whitener, G. D.; Arnold, J. *J. Chem. Soc., Dalton Trans.* **2001**, 923−927. (b) Zhang, X.; Qian, C.; Wang, C.; Zhang, Y.; Wang, Y.; Yao, Y.; Shen, Q. *Eur. J. Inorg. Chem.* **2012**, 847−858. (c) Roitershtein, D.; Domingos, Â.; Pereira, L. C. J.; Ascenso, J. R.; Marques, N. *Inorg. Chem.* **2003**, *42*, 7666−7673. (d) Müller-Buschbaum, K.; Mokaddem, Y. *Z. Anorg. Allg. Chem.* **2008**, *634*, 2360−2366.
(23) (a) Feng, X.; Liu, B.; Wang, L.-Y.; Zhao, J.-S.; Wang, J. G.; Wenig, N. S.; Shi, X.-G. *Dalton Trans.* **2010**, *39*, 8038−8049. (b) Kozieł, M.; Pełka, R.; Rams, M.; Nitek, W.; Sieklucka, B. *Inorg. Chem.* **2010**, *49*, 4268−4277. (c) Müller-Buschbaum, K.; Quitmann, C. C. *Inorg. Chem.* **2006**, *45*, 2678−2687. (d) Dubé, T.; Guan, J.; Gambarotta, S.; Yap, G. P. A. *Chem.—Eur. J.* **2001**, *7*, 374−381.
(24) (a) Thompson, L. C.; Marvin, J. R.; Bettenberg, N. C. *J. Alloys Compd.* **1992**, *180*, 229−234. (b) Carnall, W. T.; Fields, P. R.; Rajnak, K. *J. Chem. Phys.* **1968**, *49*, 4424−4442.
(25) Yin, M.; Krupa, J.-C.; Antic-Fidancev, E.; Lorriaux-Rubbens, A. *Phys. Rev. B* **2000**, *61* (12), 8073−8080.
(26) Nakazawa, E. *J. Lumin.* **1979**, *18/19*, 272−276.
(27) Ferhi, M.; Horchani-Naifer, K.; Hraiech, S.; Férid, M.; Guyot, Y.; Boulon, G. *Opt. Commun.* **2012**, *285*, 2874−2878.
(28) (a) Setlur, A. A.; Heward, W. J.; Gao, Y.; Srivastava, A. M.; Chandran, R. G.; Shankar, M. V. *Chem. Mater.* **2006**, *18*, 3314−3322. (b) van Krevel, J. W. H.; Hintzen, H. T.; Metselaar, R. *Mater. Res. Bull.* **2000**, *35*, 747−754.
(29) Blasse, G.; Grabmaier, B. C. *Luminescent Materials*; Springer Verlag: Berlin, Germany, 1994.
(30) Bachmann, V.; Ronda, C.; Meijerink, A. *Chem. Mater.* **2009**, *21*, 2077−2084.
(31) Thomas, K. S.; Singh, S.; Dieke, G. H. *J. Chem. Phys.* **1963**, *38* (9), 2180−2190.
(32) Pergolese, B.; Muniz-Miranda, M.; Bigotto, A. *J. Phys. Chem. B* **2004**, *108*, 5698−5702.
(33) Richman, I.; Satten, R. A.; Wong, E. Y. *J. Chem. Phys.* **1963**, *39*, 1833−1843.
(34) Billes, F.; Endredi, H.; Keresztury, G. *J. Mol. Struct.* **2000**, *530*, 183−200.
(35) Shionoya, S.; Yen, W. M., Eds.; *Phosphor Handbook*; CRC Press: Boca Raton, FL, 1999.